Chinese Chemical Letters 34 (2023) 107884

Contents lists available at ScienceDirect

Chinese Chemical Letters

journal homepage: www.elsevier.com/locate/cclet

Sila-annulated terrylene diimides for balanced ambipolar transporting

Kai Chen[a], Ning Xue[c], Guogang Liu[a], Yujian Liu[c], Jiajing Feng[b,*], Wei Jiang[a,c,*], Zhaohui Wang[a,c,*]

[a] Key Laboratory for Advanced Materials and Institute of Fine Chemicals, School of Chemistry & Molecular Engineering, East China University of Science and Technology, Shanghai 200237, China
[b] School of Science, China University of Geosciences (Beijing), Beijing 100083, China
[c] Key Laboratory of Organic Optoelectronics and Molecular Engineering, Department of Chemistry, Tsinghua University, Beijing 100084, China

ARTICLE INFO

Article history:
Received 11 August 2022
Revised 14 September 2022
Accepted 4 October 2022
Available online 11 October 2022

Keywords:
Terrylene diimides
Si-heteroannulation
Ambipolar transporting
Single-crystal OFETs
Organic electronics

ABSTRACT

The key building blocks, tetrachlorinated terrylene diimides and the targeted sila-annulated terrylene diimides (Si-TDIs and 2Si-TDIs) were synthesized for the first time. Single-crystal analysis verified the almost planar molecular configurations of both Si-TDIs and 2Si-TDIs. They exhibited intriguing optical properties including red-shifted absorption and near-infrared emission properties with excellent fluorescence quantum yields, as well as precisely controlled HOMO/LUMO energy levels by Si-heteroannulation. The single-crystal organic field-effect transistors based on 2Si-TDI **5a** featuring long and branched alkyl chains demonstrated well-balanced ambipolar transporting properties with electron/hole mobilities of 0.10/0.18 $cm^2\ V^{-1}\ s^{-1}$.

Ambipolar organic semiconductors, demonstrating both electron and hole transporting, have aroused considerable attention for their potential applications in flexible and low-cost organic electronic devices, such as light-emitting transistors, and complementary logic circuits [1–4]. Among them, ambipolar polymers have been extensively investigated, and high mobilities far beyond those of amorphous silicon were achieved in organic field-effect transistors (OFETs) based on polymers [5–9]. In comparison to polymers, ambipolar small molecules with excellent and balanced carrier mobilities were less reported, probably because it is difficult to achieve such narrow band gaps within a small molecular backbone [10–12]. However, organic small molecule semiconductors also possess some advantages like better synthetic reproducibility, higher crystallinity, and higher levels of purity than polymers [13,14]. Hence, it is of great significance to explore novel organic small molecule semiconductors with high and balanced ambipolar transporting performance.

Rylene diimides, consisting of oligo(*peri*–naphthalene) units and two electron-withdrawing imides, exhibit outstanding chemical and thermal stabilities, excellent charge transporting properties, and light absorbing abilities, among which perylene diimides (PDIs) are well known as one of the best n-type (electron transporting) semiconductors and widely applied to OFETs, organic photovoltaics (OPVs), as well as organic light-emitting diodes (OLEDs) [15–20]. While the research on optoelectronic properties and applications of other rylene diimides like terrylene diimides (TDIs) is relatively limited possibly due to chemical inaccessibility and solubility deficiency [21–23]. Compared with PDIs, TDIs possess specific properties, such as enhanced and red-shifted absorption spectra, and larger conjugated π-electronic systems with narrower HOMO-LUMO energy gaps [24,25]. In addition, the appropriate HOMO/LUMO energy levels of TDI are favorable for both electron and hole injection, and ambipolar transporting has been reported in TDI systems, demonstrating the great potential in ambipolar OFETs [26]. However, electron and hole mobilities of TDIs-based OFETs with the magnitude of 10^{-3} $cm^2\ V^{-1}\ s^{-1}$ leave much to be desired [27], and to the best of our knowledge, there has been no report on TDI-based ambipolar single-crystal OFETs.

We are dedicated to exploring elegantly π-extended rylene diimides derivatives with precisely controlled nanostructures and outstanding performances [28,29]. In our previous work, we developed a one-pot palladium-catalyzed Si-C bonding strategy to produce sila-annulated PDIs which have an almost planar molecular backbone, high fluorescence quantum yields, and good electron transporting properties [30]. With these advantages in mind, herein, Si-heteroannulation of TDI has been conducted. As elaborated in Fig. 1, the narrower HOMO/LUMO energy gaps of 2Si-TDI resulted from high-lying HOMO energy levels than 2Si-PDI, which is favorable for hole injection and ambipolar transporting. Thus,

* Corresponding authors.
E-mail addresses: fengjiajing@cugb.edu.cn (J. Feng), jiangwei2021@mail.tsinghua.edu.cn (W. Jiang), wangzhaohui@mail.tsinghua.edu.cn (Z. Wang).

https://doi.org/10.1016/j.cclet.2022.107884
1001-8417/

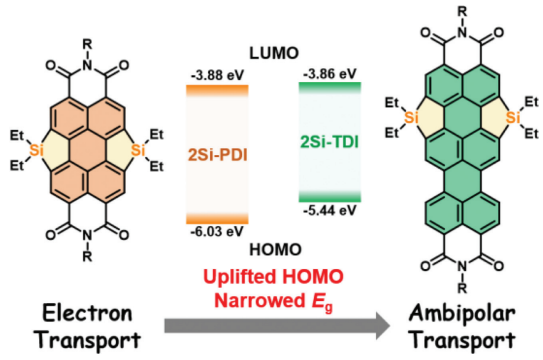

Fig. 1. A strategy to construct ambipolar transporting materials from sila-annulated PDIs (previous work) to sila-annulated TDIs (this work).

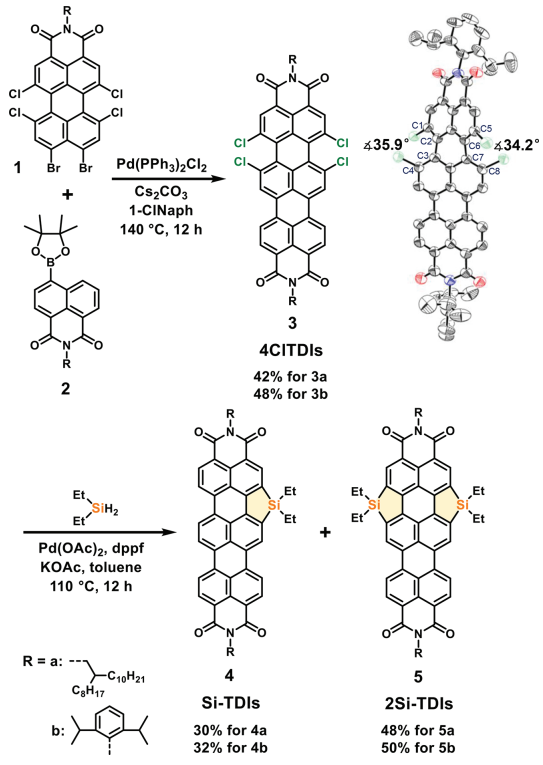

Scheme 1. The straightforward synthesis of sila-annulated terrylene diimides (**4** and **5**) and the single crystal structure of **3b**.

single-crystal OFET devices were prepared for the first time and presented well-balanced electron/hole mobilities of up to 0.10/0.18 $cm^2\ V^{-1}\ s^{-1}$ for **5a**. The introduction of silole moieties into the TDI core is expected to improve the carrier mobilities, and ethyl substituents may increase solution processability as well. Furthermore, the near-infrared emission properties with excellent fluorescence quantum yields of sila-annulated TDIs reveal the potential for further application in luminescent devices.

The synthetic route to sila-annulated TDIs is shown in Scheme 1. Firstly, 4ClTDIs (**3**) were obtained for the first time by adopting dibromo-tetrachloro-perylene monoamide **1** and 4-boronic acid pinacol ester naphthalene monoamide **2** as the starting materials, $Pd(PPh_3)_2Cl_2$ as a source of palladium, Cs_2CO_3 as base and 1-chloronaphthalene as solvent in moderate yields. It is worth noting that, compounds **3** are important building blocks for further lateral functionalization of the TDI system. The following Si-heteroannulation was carried out in the presence of diethylsilane/$Pd(OAc)_2$/dppf/KOAc at 110 °C for 12 h, affording Si-TDIs (**4**) and 2Si-TDIs (**5**) in one-pot in high overall yields. Two kinds of side chains were employed at the imide positions to regulate crystallinity and supramolecular structure. Si-TDIs (**4**) and 2Si-TDIs (**5**) show better solubility than their parent TDIs (**6**, Scheme S1 in Supporting information) benefiting from ethyl substituents on the additional silole rings and can excellently soluble in common solvents such as dichloromethane, chloroform, toluene and tetrahydrofuran at room temperature. All the targeted molecules were unambiguously confirmed by ^1H NMR and ^{13}C NMR spectroscopy, as well as HR-MALDI-TOF spectra. Thermogravimetric analysis (TGA) exhibited that they have excellent thermal stability with 5% weight loss temperatures even over 410 °C (Fig. S1 in Supporting information).

To confirm their structures, the single crystals of **3b**, **4b** and **5b** with 2,6-diisopropylphenyl substituents suitable for X-ray analysis were obtained by slow vapor diffusion of methanol into chloroform solutions. As illustrated in Scheme 1, **3b** shows a distorted configuration with dihedral angles of 35.9° for ∡C1-C2-C3-C4 and 34.2° for ∡C5-C6-C7-C8 originating from the electrostatic repulsion and steric hindrance of two chlorine atoms. Two adjacent molecules form antiparallel dimers with a torsion angle of 71.7°, producing an *S*-shaped wiggle arrangement (Fig. S2 in Supporting Information). In contrast, **4b** and **5b** revealed almost planar molecular skeletons, on account of the appropriate atomic covalent radius of the Si atom (Figs. 2a and d). In **4b**, the adjacent molecules in a column are rotated with angles of 24.3° and 58.2° to form a brick-like stacking along the *b*-axis (Figs. 2b and c). While molecules **5b** pack in an edge-to-face herringbone arrangement along the *b*-axis with a tilt angle of 65.6° (Figs. 2e and f). In both compounds, there are no π-π interactions between the adjacent TDI planes owing to the steric hindrance and electrostatic repulsion of bulky 2,6-diisopropylphenyl substituents on imide positions and ethyl groups on silicon atoms.

The absorption and emission spectra of **4** and **5** were investigated in chloroform at room temperature with the parent TDIs (**6**) for comparison. As displayed in Fig. 3a and Fig. S3a (Supporting information), all sila-annulated TDIs and parent TDIs exhibited similar absorption shapes in the region of 500–750 nm, and the lowest energy absorption peaks were attributable to vibronic π-π^* (HOMO → LUMO) transitions based on time-dependent density functional theory (TDDFT) calculations (Fig. S4 in Supporting information). Because of the σ^*-π^* hyperconjugation between the Si-C bond and π-skeleton, in conjunction with the inductive effect of ethyl substituents, the absorption maxima of sila-annulated TDIs showed gradual red-shift with the increasing number of silole rings, while the molar extinction coefficients gradually decreased. The optical energy gaps, obtained from absorption edges, were 1.83 eV for **6a**, 1.77 eV for **4a**, and 1.73 eV for **5a**, respectively. Notably, sila-annulated TDIs display excellent fluorescence emission properties with fluorescence quantum yields of 41%–44% extending to near-infrared regions covering 650–850 nm (Fig. 3b and Fig. S3b in Supporting information), implying the potential for further preparation of luminescent devices.

Cyclic voltammetry (CV) measurements were conducted in CH_2Cl_2 solutions to characterize the electrochemical properties of sila-annulated TDIs. As shown in Fig. 3c and Fig. S3c (Supporting information), sila-annulated TDIs exhibited almost the same behaviors as the parent TDI with one reversible oxidation wave and one reversible reduction wave, indicating that slight influence on electrochemical properties has been brought by embedding silole rings into the TDI skeleton. The half-wave reduction/oxidation potentials were −1.15/0.67 V for **4a**, −1.14/0.65 V for **5a**, and −1.11/0.75 V for **6a** vs. Fc/Fc^+. Estimated from the reduction/oxidation onset peaks, the LUMO/HOMO levels were calculated to be −3.89/−5.47 eV for **4a**, −3.86/−5.44 eV for **5a,** and −3.90/−5.49 eV for **6a**. The slightly uplifted LUMO/HOMO levels were owing to σ^*-π^* hyperconjuga-

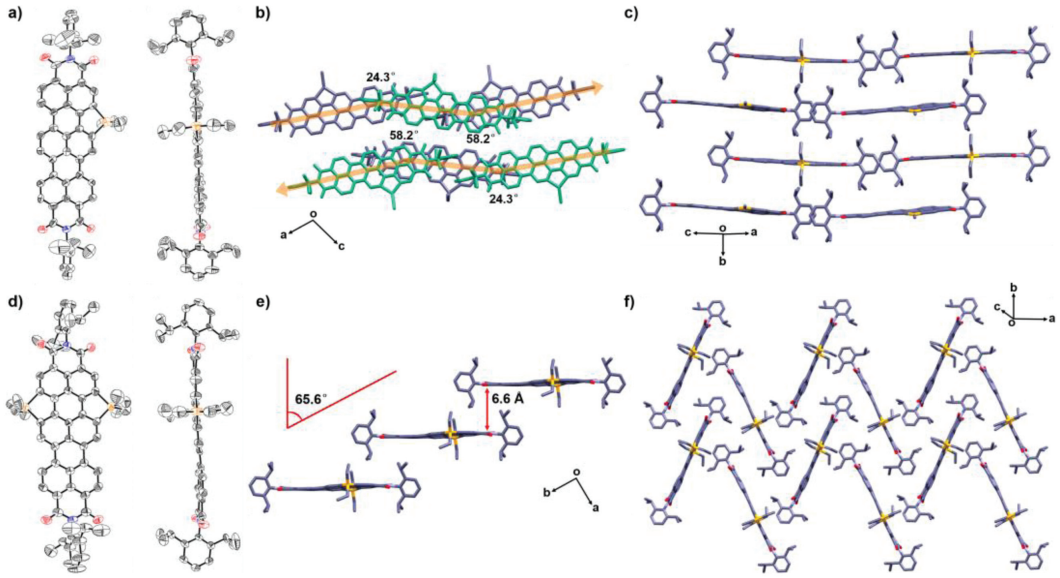

Fig. 2. Single crystal structures of **4b** and **5b**, thermal ellipsoids are set at 50% probability. Top view and side view of (a) **4b** and (d) **5b**. Arrangement view from *b*-axis for **4b** (b) and a column arrangement along the *b*-axis for **5b** (e). Packing arrangements of (c) **4b** and (f) **5b**.

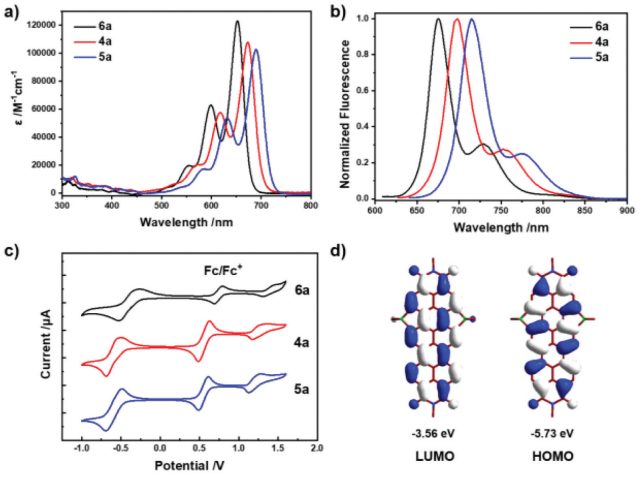

Fig. 3. (a) Absorption and (b) emission spectra of **4a**, **5a** and **6a** in $CHCl_3$ (1×10^{-5} mol/L), as well as their (c) cyclic voltammograms in CH_2Cl_2 (*vs.* Fc/Fc^+). (d) LUMO and HOMO energy levels of model 2Si-TDI (**5**).

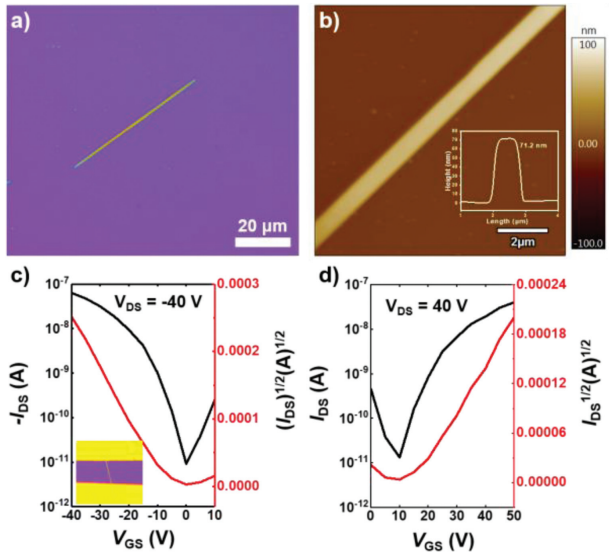

Fig. 4. (a) Optical microscopy (OM) image, and (b) Atomic force microscopy (AFM) images of **5a**. (c, d) Representative transfer characteristics of the ambipolar single-crystal OFETs based on **5a**.

tion between silole moieties and TDI backbone, in combination with inductive mechanism from ethyl donor substituents, among with the latter was dominant. Meantime, the narrowed energy gaps are attributed to the expansion of the π-systems from PDI to TDI with remarkable uplifted HOMO levels. The experimental energy levels were consistent with DFT calculations (Fig. 3d and Fig. S5 in Supporting information), and all the data on optoelectronic properties were listed in Table 1 and Table S2 (Supporting information).

We first examined the charge transporting characteristics of these sila-annulated TDIs in thin-film OFETs. Both compounds exhibited ambipolar transporting behavior. The maximal hole and electron mobilities for **4a** were 3.7×10^{-5} and 4.8×10^{-3} cm^2 V^{-1} s^{-1}, respectively, while **5a** possessed better values with the maximal hole and electron mobilities of 6×10^{-3} and 3.6×10^{-2} cm^2 V^{-1} s^{-1}, respectively. Single-crystal transistors based on **5a** were further constructed by a "gold strip" method. The optical microscopy (OM) images and atomic force microscopy (AFM) in Figs. 4a and b showed one-dimensional (1D) micrometer-sized ribbon-like crystals of **5a** with lengths of tens of micrometers and widths of several micrometers, as well as a smooth surface. The X-ray diffraction (XRD) images demonstrated sharp interlayer Bragg diffractions of microribbons (Fig. S7 in Supporting information), and the bright selected area electron diffraction (SAED) patterns in Fig. S9 (Supporting information) reflected the excellent single-crystal nature. The representative transfer characteristics of **5a**-based single-crystal OFETs measured under nitrogen conditions were depicted in Figs. 4c and d, and the corresponding characteristics were summarized in Table S4 (Supporting information). The results indicated well-balanced ambipolar transporting performances with the maximal hole and electron mobilities of 0.18 cm^2 V^{-1} s^{-1} and 0.10 cm^2 V^{-1} s^{-1}, respectively, which were the highest ambipolar mobility values of OFETs based on TDI derivatives so far.

Table 1
Optical properties and frontier orbital energy levels of Si-TDI (**4a**), 2Si-TDI (**5a**), and the parent TDI (**6a**) in solutions.

Compound	$\lambda_{max,abs}$ (nm)[a]	ε_{max} (L mol^{-1} cm^{-1})[a]	$\lambda_{max,em}$ (nm)[a]	Φ[b]	E_{LUMO} (eV)[c]	E_{HOMO} (eV)[c]	$E_{g,elec}$ (eV)[d]	$E_{g,opt}$ (eV)[e]
6a	653	123,100	675	55%	−3.90	−5.49	1.59	1.83
4a	673	108,000	698	45%	−3.89	−5.47	1.58	1.77
5a	690	102,700	715	41%	−3.86	−5.44	1.58	1.73

[a] Measurements were performed in $CHCl_3$ (1.0×10^{-5} mol/L).
[b] Absolute quantum yield.
[c] Estimated from the onset of the first reduction or oxidation peaks and calculated according to $E_{LUMO} = -(4.8 + E_{onset,cathodic})$ eV or $E_{HOMO} = -(4.8 + E_{onset,anodic})$ eV, and the $E_{onset,cathodic}$ and $E_{onset,anodic}$ values are versus Fc/Fc^+.
[d] Calculated according to $E_{g,elec}$ (eV) = E_{LUMO} - E_{HOMO}.
[e] Calculated by the onset of absorption in $CHCl_3$ solutions according to $E_{g,opt}$ (eV) = $(1240/\lambda_{onset,abs})$.

In summary, we present sila-annulated TDIs by palladium-catalyzed one-pot reactions using the key building block 4ClTDIs (**3**). Single-crystal X-ray analysis unambiguously verified the distorted structure of **3b** and the almost planar structures of sila-annulated TDIs. The absorption and emission spectra were gradually red-shifted with the increasing number of silole rings. More importantly, the single-crystal OFET devices based on **5a** exhibited well-balanced ambipolar transporting performances with electron/hole mobilities of 0.10/0.18 cm^2 V^{-1} s^{-1}, which was the highest ambipolar mobility values of OFETs based on TDI derivatives so far.

Declaration of competing interest

The authors declare that they have no known competing financial interests or personal relationships that could have appeared to influence the work reported in this paper.

Acknowledgments

This work was financially supported by the National Natural Science Foundation of China (NSFC, Nos. 21901138, 21790361 and 22122503), the Shandong Provincial Natural Science Foundation (No. ZR2019ZD50), and China Fundamental Research Funds for the Central Universities (No. 2–9–2020–041).

Supplementary materials

Supplementary material associated with this article can be found, in the online version, at doi:10.1016/j.cclet.2022.107884.

References

[1] J. Zaumseil, R.H. Friend, H. Sirringhaus, Nat. Mater. 5 (2006) 69–74.
[2] A.C. Arias, J.D. MacKenzie, I. McCulloch, J. Rivnay, A. Salleo, Chem. Rev. 110 (2010) 3–24.
[3] S.Z. Bisri, C. Piliego, J. Gao, M.A. Loi, Adv. Mater. 26 (2014) 1176–1199.
[4] J. Zaumseil, H. Sirringhaus, Chem. Rev. 107 (2007) 1296–1323.
[5] L. Yang, D.C. Wei, Chin. Chem. Lett. 27 (2016) 1395–1404.
[6] Z. Ni, H. Wang, Q. Zhao, et al., Adv. Mater. 31 (2019) 1806010.
[7] M. Kim, W.T. Park, S.A. Park, et al., Adv. Funct. Mater. 29 (2019) 1805994.
[8] Z. Yi, Y. Jiang, L. Xu, et al., Adv. Mater. 30 (2018) 1801951.
[9] Y. Gao, Y. Deng, H. Tian, et al., Adv. Mater. 29 (2017) 1606217.
[10] S.S. Cheng, P.Y. Huang, M. Ramesh, et al., Adv. Funct. Mater. 24 (2014) 2057–2063.
[11] W. Yue, T. He, M. Stolte, M. Gsänger, F. Würthnner, Chem. Commun. 50 (2014) 545–547.
[12] X. Cui, C. Xiao, T. Winands, et al., J. Am. Chem. Soc. 140 (2018) 12175–12180.
[13] R. Ozdemir, D. Choi, M. Ozdemir, et al., J. Mater. Chem. C 5 (2017) 2368–2379.
[14] Z. Wang, X. Li, Y. Zou, et al., J. Mater. Chem. C 4 (2016) 7230–7240.
[15] W. Jiang, Y. Li, Z. Wang, Acc. Chem. Res. 47 (2014) 3135–3147.
[16] X. Zhan, A. Facchetti, S. Barlow, et al., Adv. Mater. 23 (2011) 268–284.
[17] C. Schaack, A.M. Evans, F. Ng, M.L. Steigerwald, C. Nuckolls, J. Am. Chem. Soc. 144 (2022) 42–51.
[18] Y. Liu, Z. Ma, Z. Wang, W. Jiang, J. Am. Chem. Soc. 144 (2022) 11397–11404.
[19] Q. Fan, W. Ni, L. Chen, G.G. Gurzadyan, Y. Xiao, Chin. Chem. Lett. 31 (2020) 2965–2969.
[20] J.M. Wang, E.F. He, H.L. Wang, et al., Chin. Chem. Lett. 28 (2017) 383–387.
[21] L. Chen, C. Li, K. Müllen, J. Mater. Chem. C 2 (2014) 1938–1956.
[22] J. Feng, L. Fu, H. Geng, W. Jiang, Z. Wang, Chem. Commun. 56 (2020) 912–915.
[23] L. Li, J. Wang, M. Chen, et al., Chin. Chem. Lett. 30 (2019) 2254–2258.
[24] J. Feng, N. Liang, W. Jiang, et al., Org. Chem. Front. 4 (2017) 811–816.
[25] C. Jung, B.K. Müller, D.C. Lamb, et al., J. Am. Chem. Soc. 128 (2006) 5283–5291.
[26] C. Liu, Z. Liu, H.T. Lemke, et al., Chem. Mater. 22 (2010) 2120–2124.
[27] C. Liu, Y. Xu, Z. Liu, et al., Org. Electron. 15 (2014) 1884–1889.
[28] W. Jiang, Z. Wang, J. Am. Chem. Soc. 144 (2022) 14976–14991.
[29] J. Feng, Y. Wu, Q. Yu, et al., CCS Chem. 2 (2020) 271–279.
[30] Z. Ma, C. Xiao, C. Liu, et al., Org. Lett. 19 (2017) 4331–4334.